Unconventional thermoelectric behaviors and enhancement of figure of merit in Rashba spintronic systems

Cong Xiao, Dingping Li, and Zhongshui Ma
School of Physics, Peking University, Beijing 100871, China
Collaborative Innovation Center of Quantum Matter, Beijing, 100871, China

Thermoelectric transport in strongly spin-orbit coupled two-dimensional Rashba system is studied using the exact solution of the linearized Boltzmann equation. Some unusual transport behaviors are revealed. We show that the electrical conductivity takes a Drude form when the Fermi energy E_F is above the band crossing point, but a non-Drude form which is a quadratic function of E_F when E_F lies below the band crossing point. The Mott relation breaks down when E_F lies in the vicinity of the band crossing point. It is shown that the thermopower and thermoelectric figure of merit are strongly enhanced when E_F downs below the band crossing point. This enhancement is attributed to not only the one-dimensional-like density of state but also the unconventional intraband elastic scattering below the band crossing point. The differences between these results and those obtained by the relaxation time approximation are discussed in detail.

PACS numbers: 72.20.Pa, 73.50.Lw, 75.70.Tj

I. INTRODUCTION

In two-dimensional electron system (2DES) with Rashba spin-orbit coupling (SOC), when the energy downs below the band crossing point (BCP), a band valley emerges (Fig. 1) with different topology of Fermi surfaces (FS) from that when the energy is above the BCP[1–3]. In the band valley the dispersion curve is not monotonic and the density of state (DOS) is one-dimensional (1D)-like. In the case of strong SOC, the Fermi level can lie in the vicinity of or even below the BCP, and the valley structure can survive the weak disorder and thermal smearing at low temperatures. Therefore, in this case the nontrivial topology of FS in the band valley may affect the transport properties significantly.

The strongly spin-obit coupled 2DES, formed at the Te-terminated surface in layered polar semiconductors BiTeX (X=Cl, Br, I), has been discovered recently by ARPES measurements in agreement with ab-initio calculations[4–8]. In such 2DES the giant Rashba SOC coefficient is one order of magnitude higher than that in conventional III-V semiconductor heterostructures[9]. In addition, the BiTeX quantum well[10] may be another candidate to realize strongly spin-orbit coupled 2DES. Very recently the first-principle band structure calculation has suggested the strain engineering of heavy-metal film on layered large-gap semiconductor substrate[11] as a promising way to form 2DES with strong Rashba SOC, e.g., Au single layer on strained InSe(0001). In aforementioned 2DES, the large Rashba spin-splitting provides a chance to study the unconventional transport properties induced by the band valley and band crossing.

The effects of the band valley and band crossing on spin transport and superconducting electronics have received much theoretical attention, e.g., the non-Dyakonov-Perel spin relaxation behavior[12], the non-Edelstein electric-field induced spin polarization[13,14], the enhanced spin-orbit torque efficiency[2], the enhanced superconducting instabilities[1] and the specular Andreev reflection in the interface of a superconductor and a 2DES with strong Rashba SOC[15]. In addition, spin-related thermoelectric conversion in systems with strong Rashba SOC is gathering increasing attention, which is not only essential for exploring spintronics devices[16] but also important for developments of spin caloritronics[17]. For Rashba 2DES, based on the relaxation time approximation (RTA)[2,10,18] in the semiclassical Boltzmann equation (SBE) approach, it has been suggested recently that the dimensional reduction of the electronic structure from 2D to 1D can result in enhancements of the diffusive thermopower and thermoelectric figure of merit[10] $ZT = (\alpha/\sigma)^2 \sigma T/\kappa$. Here σ, α, κ and T denote the electrical conductivity, Peltier coefficient, thermal conductivity, absolute temperature, respectively. In the RTA, the enhancement of thermopower was attributed solely to the 1D-like DOS below the BCP[10].

However, so far, no fully satisfactory theoretical study on thermoelectric transport exists for the case that E_F lies in the vicinity of or below the band crossing point. This is because that the RTA is inappropriate for Rashba 2DES at low temperatures when the electron-impurity scattering dominates, in the case of strong SOC[14]. For Fermi energies above the BCP, the RTA can not handle the difference in the relative importance between the interband and intraband elastic scatterings. This difference is significant when E_F lies near the BCP, so the RTA is unsuitable for this case. While for Fermi energies below the BCP, the nontrivial FS topology induces not only the 1D-like DOS, but also nonconventional intraband scattering[14](inter-branch and intra-branch scatterings, the two branches are denoted in Fig. 1) which is also beyond the scope of RTA. It has been shown that[14], when E_F is below the BCP, the nonequilibrium spin polarization calculated by an exact transport time solution of the SBE is quite different from the result obtained by the constant RTA[13]. This motivates us to employ the exact solution[14] of the SBE to systematically study the

effects of strong Rashba SOC on the spin-related thermoelectric transport in 2DES at low temperatures.

In this paper the exact solution of the SBE is employed to calculate thermoelectric transport coefficients and the figure of merit in Rashba 2DES. This solution is suitable when electron-impurity scatterings dominate. We show that the electrical conductivity takes a Drude form when E_F is above the BCP, but a non-Drude form which is a quadratic function of E_F when E_F is below the BCP. We found that, the E_F-dependence of the Peltier coefficient is not monotonic and the Mott relation[19] breaks down in the vicinity of the BCP. It is shown that the thermopower and thermoelectric figure of merit have strong enhancements when E_F is tuned below the BCP. This enhancement in the thermoelectric performance is a combined result of the 1D-like DOS and the unconventional intraband scattering induced by the nontrivial FS topology in the band valley.

The paper is organized as follows. We present the characteristic properties of Rashba 2DES in Sec. II. The thermoelectric transport coefficients are calculated in Sec. III. In Sec. IV, the thermoelectric figure of merit is presented. The conclusions of the present paper are given in Sec. V.

II. CHARACTERISTIC PROPERTIES OF RASHBA SPINTRONIC SYSTEMS

A. The DOS and the topological features of FS

We consider a Rashba 2DES with spin-independent disorder

$$H=\frac{\mathbf{p}^2}{2m}+\frac{\beta}{\hbar}\hat{\sigma}\cdot(\mathbf{p}\times\hat{\mathbf{z}})+V(\mathbf{r}), \tag{1}$$

where $\mathbf{p}=\hbar\mathbf{k}$ is the momentum of the electron, m is the effective mass, $\hat{\sigma}=(\sigma_x,\sigma_y,\sigma_z)$ are the Pauli matrices, β the Rashba coefficient. The disorder potential $V(\mathbf{r})=\sum_i V_0\delta(\mathbf{r}-\mathbf{R}_i)$ is produced by randomly distributed identical δ-scatters at $\mathbf{R}_i$ and is modeled by the standard Gaussian disorder average $\left\langle|V_{\mathbf{k'k}}|^2\right\rangle_{dis}=n_{im}V_0^2$ where n_{im} is the impurity concentration, V_0 is the strength of the disorder potential, $V_{\mathbf{k'k}}$ is the orbital disorder matrix element and $\langle..\rangle_{dis}$ the disorder average. The inner eigenstates and eigenenergies of the clean system read $|u_{\lambda\mathbf{k}}\rangle=\frac{1}{\sqrt{2}}(1,-i\lambda\exp(i\phi))^T$ and $E_{\lambda k}=\frac{\hbar^2k^2}{2m}+\lambda\beta k$, respectively. Here $\lambda=\pm$ and ϕ is the polar angle of $\mathbf{k}$.

The DOS at energy $E\geq 0$ is given by $N_>(E)=\sum_\lambda N_\lambda(E)=2N_0$ with $N_\lambda(E)=N_0\frac{k_\lambda(E)}{k_\lambda(E)+\lambda k_R}$ the DOS in the λ band. Here $k_R=m\frac{\beta}{\hbar^2}$, $N_0=\frac{m}{2\pi\hbar^2}$, $k_\lambda(E)=-\lambda k_R+\frac{1}{\beta}\sqrt{E_R^2+2E_RE}$ is the wave number corresponding to a given energy $E\geq 0$ in the λ band, $E_R=m\left(\frac{\beta}{\hbar}\right)^2$ is the "Rashba energy".

Below the BCP there is a valley structure in the lower Rashba band, with the bottom located at k_R and the minimal energy $E_-(k_R)=-\frac{1}{2}E_R$. At a given energy E in the band valley above the bottom, there are two wave numbers $k_{-\nu}(E)=k_R+(-1)^{\nu-1}\frac{1}{\beta}\sqrt{E_R^2+2E_RE}$ where $\nu=1,2$ denote the two monotonic branches as shown in Fig. 1. It is worth noticing that the group velocity in the -2 branch is anti-parallel to the momentum. The DOS in this regime has a 1D behavior $N_<(E)=\sum_{\nu=1}^2 N_{-\nu}(E)=2N_0\frac{E_R}{\sqrt{E_R^2+2E_RE}}$ with $N_{-\nu}(E)=N_0\frac{k_{-\nu}(E)}{|k_{-\nu}(E)-k_R|}$.

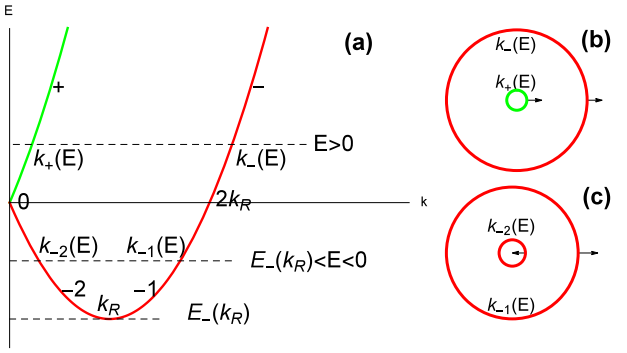

FIG. 1. Band structure of the Rashba 2DES. (a) Dispersion curve. The energy of the bottom of the dispersion curve is $E_-(k_R)=-\frac{1}{2}E_R$ with $k_R=m\frac{\beta}{\hbar^2}$. At a given energy $E\geq 0$, the wave number in $\pm$ band is defined as $k_\pm(E)$. For $-\frac{1}{2}E_R<E\leq 0$, there are two monotonic regions on $E-k$ curve: the one from $k=0$ to k_R is marked by the branch -2, whereas the other from $k=k_R$ to $2k_R$ marked by branch -1. The wave number $k_{-\nu}(E)$ represents the wave number in the $-\nu$ branch at given E, where $\nu=1,2$. (b) Constant-energy circles for $E>0$. (c) Constant-energy circles for $-\frac{1}{2}E_R<E<0$. The arrows in (b) and (c) represent the directions of the group velocity.

B. The response to the external electric field and temperature gradient

In the linear response regime, within the semiclassical Boltzmann framework the electric current density $\mathbf{j}^e$ and heat current density $\mathbf{j}^h$ are given by

$$\mathbf{j}^e=e\sum_l f_l\mathbf{v}_l\equiv\sigma\mathbf{E}^*+\alpha(-\nabla T) \tag{2}$$

and

$$\mathbf{j}^h=\sum_l f_l\mathbf{v}_l(E_l-\mu)\equiv T\alpha\mathbf{E}^*+\kappa(-\nabla T). \tag{3}$$

Here l is the eigenstate index, $\mathbf{v}_l$ is the group velocity of state l, f_l denotes the semiclassical distribution function (DF) for the electron wave packets, $\mathbf{E}^*=\mathbf{E}-\frac{1}{e}\nabla\mu$ the gradient of the electrochemical potential, ∇T the temperature gradient. $f_l=f^0(E_l)+g_l$ where f^0 is the equilibrium Fermi-Dirac DF and g_l the out-of-equilibrium deviation linear in the generalized driven force. The system is

time-reversal invariant, thus the Hall transport is absent and σ, α, κ are all numbers. To calculate these thermoelectric transport coefficients in low temperature cases where the static impurity scattering dominates, we employ the SBE[19]. In the presence of weak uniform electric field and gradients of chemical potential and temperature, the linearized SBE suitable for the present system in nonequilibrium stationary state takes the form[19,20]:

$$\mathbf{F}_l \cdot \mathbf{v}_l \frac{\partial f^0}{\partial E_l} = -\sum_{l'} \omega_{l',l} \left[g_l - g_{l'} \right]. \tag{4}$$

Here $\mathbf{F}_l = e\mathbf{E}^* + \frac{E_l - \mu}{T}(-\nabla T)$ is the generalized force acting on state l. $\omega_{l',l}$ is the elastic scattering rate from eigenstate l to l', which can be obtained by the golden rule in quantum mechanical scattering theory. For the present system, the Born approximation in the lowest order is sufficient[20,21], i.e., $\omega_{l',l} = \frac{2\pi}{\hbar}\left\langle \left|V_{\mathbf{k'k}}\right|^2 \right\rangle_{dis} \left|\langle u_{l'}|u_l\rangle\right|^2 \delta\left(E_l - E_{l'}\right)$.

The SBE in isotropic 2D Rashba system can be solved conveniently using energy E and polar angle ϕ and band index λ as variables, i.e., $l = (E, \lambda, \phi)$. While the valley region of the lower band is worth noticing due to the non-monotonic band dispersion. In the valley region, the branch index $-\nu$ introduced above is needed to denote the eigenstate, i.e., $l = (E, -\nu, \phi)$. Then the exact solution of Eq. (4) can be obtained, which we refer to our previous work[14]:

$$g_\lambda(E) = \left(-\partial_E f^0\right) \mathbf{F}_E \cdot \frac{\hbar \mathbf{k}_\lambda(E)}{m} \tau \tag{5}$$

when $E > 0$, and

$$g_{-\nu}(E) = \left(-\partial_E f^0\right) \mathbf{F}_E \cdot \frac{\hbar \mathbf{k}_{-\nu}(E)}{m} \tau (-1)^{\nu-1} \frac{E_R^2 + 2E_R E}{E_R^2} \tag{6}$$

when $E_-(k_R) < E < 0$. Here $\mathbf{F}_E$ represents the generalized force acting on electrons with energy E, $\tau = \left(\frac{2\pi n_{im} V_0^2 N_0}{\hbar}\right)^{-1}$ is the ordinary momentum relaxation time. At $E = 0$, $g_+(E \to 0^+) = g_{-2}(E \to 0^-) = 0$, $g_{-1}(E \to 0^-) = g_-(E \to 0^+)$. The DOS at $(E = 0, k = 0)$ vanishes, so this point does not contribute to transport quantities in Eq. (2) and (3), and only the outer constant-energy circle $(E = 0, k = 2k_R)$ contributes at $E = 0$.

We note that Eq. (5) takes into account the intraband $(\lambda \to \lambda)$ and interband $(\lambda \to -\lambda)$ elastic scatterings. While Eq. (6) takes into account the unconventional intraband scattering in the band valley, i.e., the intra-branch $(-\nu \to -\nu)$ and inter-branch $(-\nu \to -(3-\nu))$ elastic scatterings.

C. The chemical potential at low temperatures

The relation between E_F and μ is needed for investigating the E_F-dependence of Peltier coefficient and thermal conductivity. It can be obtained by considering the electron density as follows. At finite temperatures, the electron density can be calculated by $n_e \equiv n_e^> + n_e^<$, where we define $n_e^>$ and $n_e^<$ as

$$\begin{aligned} n_e^> &= \int_0^\infty dE f^0(E) N_>(E), \\ n_e^< &= \int_{E_-(k_R)}^0 dE f^0(E) N_<(E). \end{aligned} \tag{7}$$

By defining two functions:

$$Q_>(E) = \int_0^E dE' N_>(E') = 2N_0 E \tag{8}$$

for $E \geq 0$ and

$$Q_<(E) = \int_E^0 dE' N_<(E') = 2N_0 E_R \left(1 - \sqrt{1 + 2\frac{E}{E_R}}\right) \tag{9}$$

for $E \leq 0$, $n_e^>$ and $n_e^<$ can be written in the following forms via integration by parts:

$$\begin{aligned} n_e^> &= \int_0^\infty dE \left(-\frac{\partial f^0}{\partial E}\right) Q_>(E), \\ n_e^< &= Q_<(E_-(k_R)) - \int_{E_-(k_R)}^0 dE \left(-\frac{\partial f^0}{\partial E}\right) Q_<(E). \end{aligned} \tag{10}$$

Setting

$$\frac{E - \mu}{k_B T} = x, \frac{\mu}{k_B T} = -t_1, \frac{E_F}{k_B T} = -t_2, \tag{11}$$

in Eq. (10) and restricting to not too low chemical potential $\frac{\mu - E_-(k_R)}{k_B T} \gg 1$, the total electron density is found as

$$\begin{aligned} \frac{n_e}{2N_0 E_R} &= \int_{t_1}^\infty dx \left(-\frac{\partial f^0}{\partial x}\right) \left[(x - t_1)\frac{k_B T}{E_R} + 1\right] \\ &+ \int_{-\infty}^{t_1} dx \left(-\frac{\partial f^0}{\partial x}\right) \sqrt{1 + 2(x - t_1)\frac{k_B T}{E_R}}. \end{aligned} \tag{12}$$

Here the condition $\frac{\mu - E_-(k_R)}{k_B T} \gg 1$ can be realized at low temperatures due to the giant Rashba SOC, e.g., in BiTeI surface state[8] $E_-(k_R) \simeq -90meV$, if $\mu = \frac{1}{2}E_-(k_R)$ we have $\frac{\mu - E_-(k_R)}{k_B} \simeq 450K$. At zero-temperature $\mu = E_F$, when $E_F \geq 0$ it has been obtained that[22] $n_e(E_F \geq 0) = 2N_0(E_F + E_R)$. While when $E_F \leq 0$ we obtain

$$n_e(E_F \leq 0) = \int_{k_{-2}(E_F)}^{k_{-1}(E_F)} \frac{kdk}{2\pi} = 2N_0\sqrt{E_R^2 + 2E_R E_F}. \tag{13}$$

In this case the Fermi level intersects only the lower band and only the annulus lying between the two Fermi circles of radii $k_{-1,-2}(E_F)$ is filled. This nontrivial topology of Fermi surfaces in the band valley has been highlighted in previous researches[1–3]. Substituting the electron density

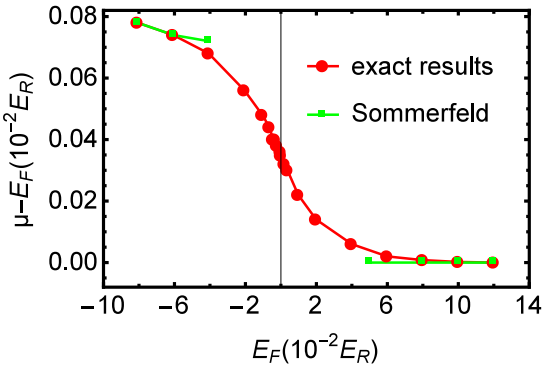

FIG. 2. The difference between the chemical potential and the Fermi energy. The temperature is fixed to $0.02E_R/k_B$. The numerical results describe exactly the behavior near $E_F = 0$, which is beyond the scope of the Sommerfeld expansion.

into Eq. (12), we obtain the Fermi energy dependence of chemical potential at a given temperature, as presented in Fig. 2.

When $E_F \geq 0.1E_R$, $\mu - E_F = 0$, same as the analytic result based on the Sommerfeld expansion[19] in the case of $E_F \gg k_BT$. When $E_F \leq -0.08E_R$, numerical results can be well fitted by the formula $\mu - E_F = \frac{\pi^2}{6}\frac{(k_BT)^2}{E_R+2E_F}$ obtained by the Sommerfeld expansion in the case of $-E_F \gg k_BT$ and $E_F + \frac{1}{2}E_R \gg k_BT$ (this latter condition ensures that the band valley structure and Fermi surface are not smeared out by thermal broadening and can be satisfied at low temperatures with giant Rashba SOC). It is well-known that at low temperatures in three-dimensional (3D) parabolic 2DES $\mu < E_F$, in 2D $\mu = E_F$ and in 1D $\mu > E_F$, due to different energy dependencies of the DOS[19]. Here the above two limiting cases correspond to 2D and 1D cases, due to the 2D- and 1D-like DOS for energies above and below the BCP, respectively.

When E_F is in the intermediate region $-0.08E_R \leq E_F \leq 0.1E_R$, the Sommerfeld expansion is not valid and numerical results clearly show continuous transition between above two limiting cases. This transition from 2D to 1D is resulted by the Fermi surfaces topology change in Rashba model.

III. THERMOELECTRIC RESPONSE COEFFICIENTS

A. Drude-like and non-Drude forms of electrical conductivities

In what follows we assume that the generalized force is applied in x direction. When both bands are partially occupied, the zero-temperature electrical conductivity is calculated by substituting the group velocity $\mathbf{v}(E,\lambda,\phi) = \frac{N_0}{N_\lambda(E)}\frac{\hbar\mathbf{k}_\lambda(E)}{m}$ and the DF Eq. (5) into Eq. (2). The result is

$$\sigma(E_F \geq 0) = \frac{e^2}{2\pi^2\hbar}\frac{2\pi(E_F+E_R)\tau}{\hbar}, \tag{14}$$

where and below we use the notation $\sigma(E_F)$ to represent the zero-temperature electrical conductivity $\sigma(T=0,E_F)$ for brevity.

This result still has the usual form of Drude formula $\sigma = n_e e^2\tau/m$. It has been obtained in some earlier works based on the Green's function calculation in the ladder approximation[22] or the same exact solution to the SBE[23] as our Eq. (5) when $E_F \geq 0$. In this case it looks as if the electric current were generated by charge carriers of one type with density n_e and mobility $e\tau/m$.

For Fermi energies below the BCP, substituting $g_{-\nu}$ and the group velocity $\mathbf{v}(E,-\nu,\phi) = (-1)^{\nu-1}\frac{N_0}{N_{-\nu}(E)}\frac{\hbar\mathbf{k}_{-\nu}(E)}{m}$ into Eq. (2), we obtain the zero-temperature electrical conductivity

$$\sigma(E_F \leq 0) = \frac{e^2}{2\pi^2\hbar}\frac{2\pi(E_F+E_R)\tau}{\hbar}\frac{E_R^2+2E_RE_F}{E_R^2}. \tag{15}$$

It has a quadratic dependence on the Fermi energy and does not take the form of Drude conductivity, different from Eq. (14). Since the Fermi surfaces topology in the band valley differs from that above the BCP, the behaviors of electrical conductivities are different between the two regions.

B. The Peltier coefficient

The Peltier coefficient and the electrical conductivity are connected by (details in the Appendix)

$$\alpha = \frac{1}{e}\int_{E_-(k_R)}^{\infty} dE\left(-\frac{\partial f^0}{\partial E}\right)\frac{E-\mu}{T}\sigma(E), \tag{16}$$

where $\sigma(E)$ represents the zero-temperature electrical conductivity with Fermi energy E. Usually, this energy integration is worked out by performing the Sommerfeld expansion[19]. When the Sommerfeld expansion is valid, the Mott relation holds. The former demands that $\sigma(E)$ is continuously differentiable at the chemical potential. However, according to Eqs. (14) and (15), $\sigma(E)$ takes different forms between the two sides of the BCP. Therefore $\frac{\partial\sigma(E)}{\partial E}|_\mu$ is not continuous and the Sommerfeld expansion is not valid at $\mu = 0$, thus the Mott relation fails for chemical potentials near the BCP.

Substituting Eqs. (14) and (15) into Eq. (16), we obtain the Peltier coefficient as

$$\alpha = \frac{\pi^2k_B^2T}{3e}\frac{\sigma(0)}{E_R}3\left\{1-2\frac{b(t_1)-t_1a(t_1)}{\pi^2} - \frac{2}{\pi^2}\left[c(t_1)+2t_1\left(\frac{\pi^2}{3}-b(t_1)\right)+t_1^2a(t_1)\right]\frac{k_BT}{E_R}\right\}, \tag{17}$$

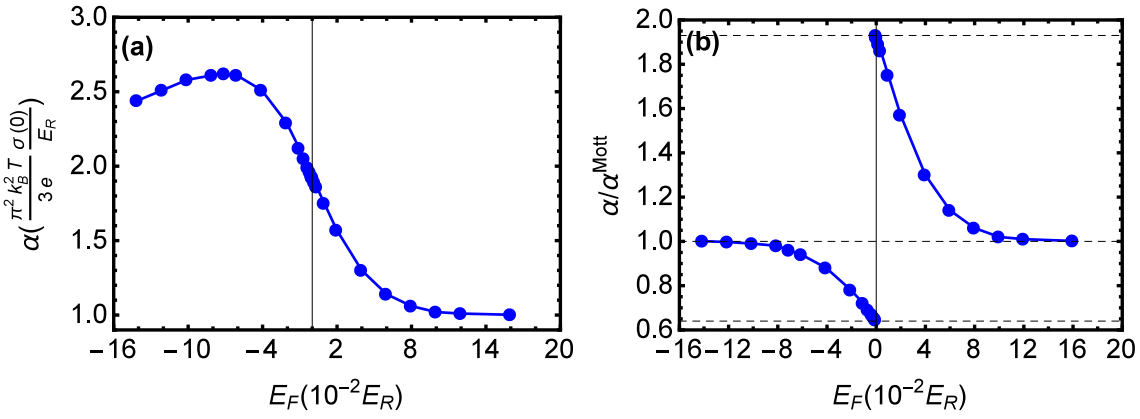

FIG. 3. (a) The Fermi energy dependence of the Peltier Coefficient. (b) The comparison between the numerical results and the Mott relation. The deviation from the Mott relation is significant when the Fermi energy lies near the BCP $E_F = 0$. In (a) and (b), the temperature is fixed to $0.02E_R/k_B$. The relation between the chemical potential and Fermi energy shown in figure 2 has been taken into account

where we define

$$a(t_1) = \int_{t_1}^{\infty} dx \left(-\frac{\partial f^0}{\partial x}\right) x,$$
$$b(t_1) = \int_{t_1}^{\infty} dx \left(-\frac{\partial f^0}{\partial x}\right) x^2, \quad (18)$$
$$c(t_1) = \int_{t_1}^{\infty} dx \left(-\frac{\partial f^0}{\partial x}\right) x^3.$$

Eq. (17) can describe the behavior of α for Fermi energies near the BCP. Because the Sommerfeld expansion is unsuitable in the band crossing region, we have to perform numerical calculations.

For temperature at $0.02E_R/k_B$, the E_F-dependence of Peltier coefficient is shown in Fig. 3(a). We find that when $E_F/E_R \geq 0.1$, α is almost constant with respect to E_F, which is consistent with the Mott relation (Eq. (19)); when $E_F/E_R \leq -0.08$, α has a nearly linear dependence on E_F, which is also consistent with the Mott relation (Eq. (20)). Between above two regions, a non-monotonic Fermi energy dependence of α in the band crossing region is found.

We use the notation α^{Mott} to denote the Peltier coefficient obtained by the Mott relation $\alpha^{Mott} = \frac{\pi^2 k_B^2 T}{3e}\frac{\partial\sigma(E)}{\partial E}|_{E=E_F}$:

$$\alpha^{Mott} = \frac{\pi^2 k_B^2 T}{3e}\frac{\sigma(0)}{E_R}, E_F \geq 0, \quad (19)$$

and

$$\alpha^{Mott} = \frac{\pi^2 k_B^2 T}{3e}\sigma(0)\frac{3}{E_R}\left[1 + \frac{4}{3}\frac{E_F}{E_R}\right], E_F \leq 0. \quad (20)$$

Combining Eq. (17) with Eqs. (19) and (20), we plot α/α^{Mott} in Fig. 3(b). When $-0.08E_R \leq E_F \leq 0.1E_R$, our results show deviations from the Mott relation.

The Mott relation fails near the BCP due to the fact that the electrical conductivity takes different forms on the two sides of the BCP. Therefore the deviation from Mott relation can be regarded as a consequence of the topological change of FS varying across the BCP.

C. The thermal conductivity

The thermal current response to the temperature gradient can be obtained by (details in the Appendix)

$$\kappa = \left(\frac{k_B}{e}\right)^2 T \int_{E_-(k_R)}^{\infty} dE \left(-\frac{\partial f^0}{\partial E}\right)\left(\frac{E-\mu}{k_B T}\right)^2 \sigma(E). \quad (21)$$

Substituting Eqs. (14) and (15) into Eq. (21), we obtain

$$\frac{\kappa}{L_0\sigma(0)T} = 1 - \frac{2c(t_1) + t_1\left(\pi^2 - 2b(t_1)\right)}{\pi^2/3}\frac{k_B T}{E_R} + \frac{\frac{7\pi^4}{15} - d(t_1) + 2t_1 c(t_1) + t_1^2\left(\frac{\pi^2}{3} - b(t_1)\right)}{\pi^2/6}\left(\frac{k_B T}{E_R}\right)^2, \quad (22)$$

where $L_0 = \frac{1}{3}\left(\frac{\pi k_B}{e}\right)^2$ is the free-electron Lorentz number, and $d(t_1) = \int_{t_1}^{\infty} dx \left(-\frac{\partial f^0}{\partial x}\right) x^4$. This is our main result for κ.

The E_F-dependence of κ is given in Fig. 4(a). It shows monotonic dependence on the Fermi energy of κ.

We compare our numerical results with that given by the Wiedemann-Franz law in Fig. 4(b). Here κ^{WF} denotes the thermal conductivity based on the Wiedemann-Franz law $\kappa^{WF} = LT\sigma(\mu) \simeq LT\sigma(E_F)$. The deviation from Wiedemann-Franz law is very slight: $\left|\frac{\kappa-\kappa^{WF}}{\kappa^{WF}}\right| <$ 6% in the whole regime we investigate here. Hence the Wiedemann-Franz law holds quite well. The difference between the validity of the Mott relation and the Wiedemann-Fran law in the band crossing region can

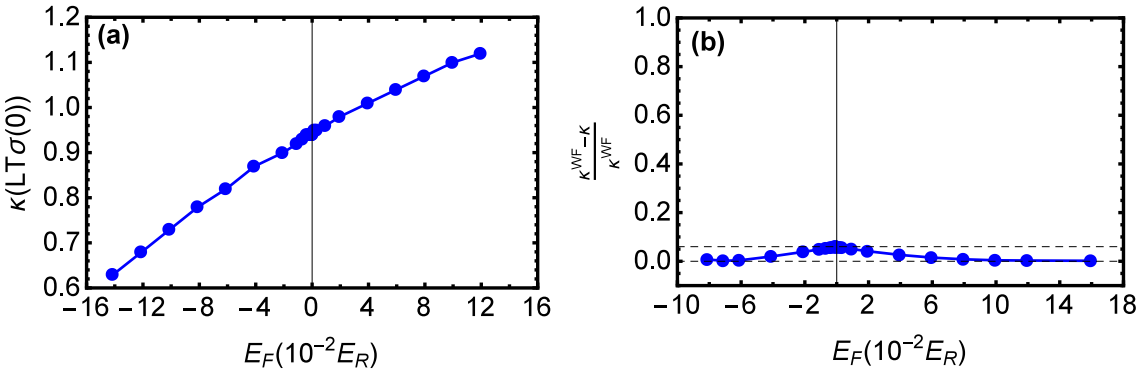

FIG. 4. (a) The Fermi energy dependence of the thermal conductivity. (b) The comparison between the numerical results and the Wiedemann-Franz law. The deviation is very slight, about $< 6\%$ near the BCP. In (a) and (b), the temperature is fixed to $0.02E_R/k_B$.

be understood as follows. The Mott relation connects the Peltier coefficient with the energy derivative of the electrical conductivity, while the Wiedemann-Franz law connects the thermal conductivity with the electrical conductivity itself. At the BCP, the electrical conductivity is continuous, but its energy derivative is not. The Peltier coefficient based on the Mott relation is not continuous across BCP. Therefore, in the vicinity of the BCP the Mott relation breaks down, while the Wiedemann-Franz law is satisfied quite well.

D. Comparison with RTA results

Eqs. (14) and (15) are different from the electrical conductivities obtained by employing the constant RTA[2]:

$$\sigma^{RTA}\left(E_F \geq 0\right) = \frac{e^2}{2\pi^2\hbar}\frac{2\pi\left(E_F+\frac{1}{2}E_R\right)\tau}{\hbar},$$
$$\sigma^{RTA}\left(E_F \leq 0\right) = \frac{e^2\tau}{2\pi\hbar^2}\sqrt{E_R^2+2E_RE_F}. \qquad (23)$$

The RTA result neither takes the Drude form for $E_F \geq 0$ nor has a polynomial dependence on E_F/E_R for $E_F \leq 0$. When $E_F \geq 0$, σ^{RTA} tends to Eq. (14) for weak SOC $E_F \gg E_R$. For Fermi energies near the BCP, the electrical conductivity obtained by the constant RTA significantly differs from Eqs. (14) and (15): $\sigma\left(E_F=0\right) = n_e\left(E_F=0\right)e^2\tau/m = 2\sigma^{RTA}\left(E_F=0\right)$. For E_F below the BCP, as long as the band valley structure can survive the thermal smearing and disorder broadening: $E_R \gg k_BT$, $\hbar/\tau$, the difference between Eq. (15) and σ^{RTA} can not be ignored.

These differences between our results and the RTA results can be understood as follows. When E_F lies high above the BCP $E_F \gg E_R$, $N_+\left(E_F\right) \simeq N_-\left(E_F\right)$, the intraband and interband scattering events are of equal importance for both the inner (+) and outer (-) Fermi circles. Only in this case the RTA works well. When E_F lies near the BCP, $N_+\left(E_F\right)$ tends to zero. Thus, for Fermi electrons on the inner Fermi circle the interband scattering events dominate over the intraband scattering[24]; while for Fermi electrons on the outer Fermi circle the intraband scattering events dominate over the interband scattering. The difference in the relative importance between the intraband and interband scattering events as well as its change with varying E_F can not be described by the RTA. When E_F lies below the BCP, the non-Drude form of σ^{RTA} $(E_F<0)$ is caused only by the 1D-like DOS below the BCP, while that of Eq. (15) based on the exact solution of SBE relies on not only the 1D-like DOS but also the unconventional intraband scattering (inter-branch and intra-branch scatterings) induced by the nontrivial FS topology.

Now we examine the thermopower in the "Mott relation regimes": $S=\alpha^{Mott}/\sigma$. When $E_F \gg k_BT$

$$S = \frac{\pi^2k_B^2T}{3e}\frac{1}{E_F+E_R} = \frac{\pi^2k_B^2T}{3e}\frac{2N_0}{n_e} \qquad (24)$$

and when $-E_F \gg k_BT$

$$S = \frac{\pi^2k_B^2T}{3e}\frac{3}{E_R}\frac{1+\frac{4}{3}\frac{E_F}{E_R}}{\left(1+\frac{E_F}{E_R}\right)\left(1+2\frac{E_F}{E_R}\right)}. \qquad (25)$$

The thermopower is enhanced in the band valley, similar to the thermoelectric figure of merit which will be discussed in the next section (Eqs. (27)). Eqs. (24) and (25) are different from those obtained by the constant RTA[10]:

$$S^{RTA}\left(E_F \gg k_BT\right) = \frac{\pi^2k_B^2T}{3e}\frac{1}{E_F+\frac{1}{2}E_R},$$
$$S^{RTA}\left(-E_F \gg k_BT\right) = \frac{1}{2}\frac{\pi^2k_B^2T}{3e}\frac{1}{E_F+\frac{1}{2}E_R}. \qquad (26)$$

Based on the RTA result Eq. (26), it had been concluded that below the BCP the enhancement of thermopower in a Rashba 2DES compared to a parabolic 2DES with the same electron density is caused solely by the much lower

E_F. And this lower Fermi energy is a consequence of the 1D-like DOS[10]. However, Eq. (25) obtained using the exact solution of the SBE shows that the enhancement of thermopower is a combined result of the 1D-like DOS and the unconventional inter-branch and intra-branch scatterings in the band valley.

In conventional semiconductor asymmetric quantum-wells the difference between Eq. (14) and the 1st equation of Eq. (23) is negligible due to the weak Rashba SOC $E_F \gg E_R$, so does the difference between Eq. (24) and the 1st equation of Eq. (26). In Rashba semiconductors BiTeX (X=Cl, Br, I), despite that the reported Fermi levels in existing experiments are still in 3D bulk conduction band (BCB), the validity of constant RTA analysis of electrical conductivity has been questioned when E_F lies near the BCP of BCB[24]. With further studies on systematic doping in these Rashba semiconductors[24,25], it is promising that the Fermi level can be tuned into the bulk band gap. In addition, the BiTeX quantum well[10] is another possible candidate to realize strongly spin-orbit coupled 2DES. Very recently the first-principle calculation has suggested the formation of 2DES with large Rashba SOC by strain engineered growth of a Au single layer on the layered large band-gap semiconductor InSe(0001) substrate[11]. Future studies of the strain engineering of heavy-metal film on layered large-gap semiconductor substrate may also realize 2DES with stronger Rashba SOC. In these systems the transport properties of the 2DES with strong Rashba SOC can be detected experimentally and our theoretical results can be tested. For the experimental measurements of the low-temperature diffusive thermopower, the hot-electron thermocouple technique could be applied, which is much less sensitive to phonon-drag effects than conventional methods[26].

IV. THE THERMOELECTRIC FIGURE OF MERIT AND THE ENHANCEMENT BELOW THE BCP

The performance of a thermoelectric material is determined by the figure of merit $ZT = (\alpha/\sigma)^2 \sigma T/\kappa$.

For the case that the Fermi energy lies near the BCP, the ZT is shown in Fig. 5. It shows that when the Fermi energy is tuned across the BCP from $E_F = 0.1E_R$ down to $E_F = -0.08E_R$, the figure of merit acquires a strong enhancement.

When $E_F/E_R \geq 0.1$ or $E_F/E_R \leq -0.08$, the Mott relation holds very well, thus ZT can be calculated using α^{Mott}, yielding $ZT = \left(\alpha^{Mott}/\sigma\right)^2/L$, i.e.,

$$ZT = \begin{cases} \frac{\pi^2}{3}\left(\frac{k_BT}{E_R}\right)^2 \frac{1}{\left(1+\frac{E_F}{E_R}\right)^2}, E_F \gtrsim 0.1E_R \\ \frac{\pi^2}{3}\left(\frac{k_BT}{E_R}\right)^2 \frac{\left(3+4\frac{E_F}{E_R}\right)^2}{\left(1+\frac{E_F}{E_R}\right)^2\left(1+2\frac{E_F}{E_R}\right)^2}, E_F \lesssim -0.08E_R \end{cases} \quad (27)$$

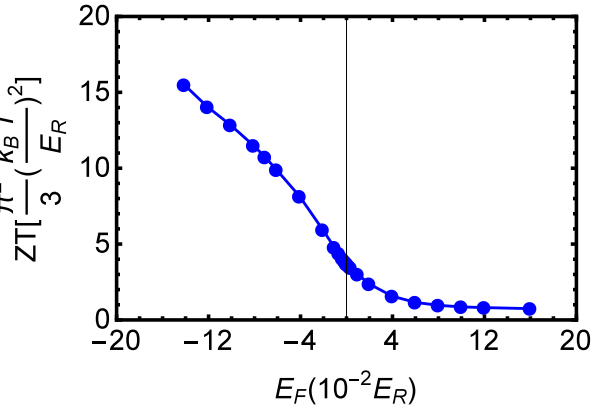

FIG. 5. The Fermi energy dependence of the figure of merit ZT when the temperature is fixed to $0.02E_R/k_B$.

In both energy intervals, ZT monotonically increases with decreasing Fermi energy, similar to the case when $-0.08 \leq E_F/E_R \leq 0.1$ shown in Fig. 5.

This enhancement in ZT when E_F is tuned below the BCP is directly related to the enhanced Peltier coefficient and the decreased electrical conductivity when E_F varies below the BCP, as shown in Fig. 3(a) and Eqs. (14) and (15). Because the Peltier coefficient is connected with the electrical conductivity , the enhancement in ZT can be attributed to the nontrivial topology of Fermi surfaces in the band valley regime.

V. CONCLUSIONS

We have calculated thermoelectric transport coefficients and the figure of merit in strongly spin-orbit coupled Rashba 2DES with spin independent disorder using the exact solution of the linearized Boltzmann equation. At low temperatures the static impurity scattering dominates, it is shown that the electrical conductivity takes a Drude form when the Fermi energy E_F is above the band crossing point, but a non-Drude form which is a quadratic function of E_F for Fermi energies below the band crossing point. This is attributed to the different topologies of Fermi surfaces on the two sides of the band crossing point. For Fermi energies near the band crossing point, the E_F-dependence of the Peltier coefficient is not monotonic, and the Mott relation breaks down. While the thermal conductivity is monotonically increasing as a function of E_F and the Wiedemann-Franz law holds quite well. The thermopower and figure of merit are strongly enhanced when E_F downs below the band crossing point. This enhancement is caused not only by the 1D-like density of state but also by the unconventional intraband elastic scattering below the band crossing point.

Our results differ from previous ones obtained by the relaxation time approximation, especially for Fermi energies in the vicinity of and below the band crossing point in systems with strong Rashba spin splitting. For Fermi

energies above the band crossing point, our results can handel the difference in the relative importance between the interband and intraband elastic scattering events, in contrast to the relaxation time approximation. This difference is significant when E_F lies in the vicinity of the band crossing point. For Fermi energies below the band crossing point, our results take into account the unconventional intraband scattering induced by the nontrivial FS topology, which can not be described by the relaxation time approximation.

Our theoretical results may be tested in strongly spin-orbit coupled 2DES, e.g., the surface state of polar semiconductors BiTeX (X=Cl, Br, I) and BiTeX quantum wells, as well as the 2DES formed by the strain engineering of heavy-metal film on layered large-gap semiconductor substrate[11].

ACKNOWLEDGMENTS

The authors are thankful for the support of NSFC (No.11274013 and No.11274018) and NBRP of China (2012CB921300).

Appendix A: Derivations of the analytic formulas for the Peltier coefficient and thermal conductivity

In order to establish the connection between the electrical conductivity and Peltier coefficient and thermal conductivity, only the original transport time form of g_l is needed, i.e.,

$$g_\lambda(E) = \left(-\frac{\partial f^0}{\partial E}\right) \mathbf{F}_E \cdot \mathbf{v}(E,\lambda,\phi)\,\tau_\lambda(E), \tag{A1}$$

and

$$g_{-\nu}(E) = \left(-\frac{\partial f^0}{\partial E}\right) \mathbf{F}_E \cdot \mathbf{v}(E,-\nu,\phi)\,\tau_{-\nu}(E), \tag{A2}$$

(In this model $\tau_\lambda(E) = \tau\frac{N_\lambda(E)}{N_0}$ and $\tau_{-\nu}(E) = \tau\frac{N_{-\nu}(E)}{N_0}\frac{E_R^2+2E_RE}{E_R^2}$, which has been included in and can be read out from the specific form of nonequilibrium DF in the paper. However, for the purpose in this supplementary material, this specific form is not needed.) Substituting Eqs. (A1) and (A2) into the two linear response equations, since the generalized force is applied in x direction, the the electrical conductivity is given by $\sigma = \sigma^> + \sigma^<$, where

$$\sigma^> = e^2 \int \frac{d\phi}{2\pi} \int_0^\infty dE \left(-\frac{\partial f^0}{\partial E}\right) \times \sum_\lambda N_\lambda(E)\, v_x^2(E,\lambda,\phi)\,\tau_\lambda(E) \tag{A3}$$

and

$$\sigma^< = e^2 \int \frac{d\phi}{2\pi} \int_{E_-(k_R)}^0 dE \left(-\frac{\partial f^0}{\partial E}\right) \times \sum_\nu N_{-\nu}(E)\, v_x^2(E,-\nu,\phi)\,\tau_{-\nu}(E). \tag{A4}$$

And the Peltier coefficient is given by $\alpha = \alpha^> + \alpha^<$ with

$$\alpha^> = e \int \frac{d\phi}{2\pi} \int_0^\infty dE \left(-\frac{\partial f^0}{\partial E}\right) \frac{E-\mu}{T} \times \sum_\lambda N_\lambda(E)\, v_x^2(E,\lambda,\phi)\,\tau_\lambda(E) \tag{A5}$$

and

$$\alpha^< = e \int \frac{d\phi}{2\pi} \int_{E_-(k_R)}^0 dE \left(-\frac{\partial f^0}{\partial E}\right) \frac{E-\mu}{T} \times \sum_\nu N_{-\nu}(E)\, v_x^2(E,-\nu,\phi)\,\tau_{-\nu}(E). \tag{A6}$$

The thermal conductivity is found as $\kappa = \kappa^> + \kappa^<$ with

$$\kappa^> = \int \frac{d\phi}{2\pi} \int_0^\infty dE \left(-\frac{\partial f^0}{\partial E}\right) \frac{(E-\mu)^2}{T} \times \sum_\lambda N_\lambda(E)\, v_x^2(E,\lambda,\phi)\,\tau_\lambda(E) \tag{A7}$$

and

$$\kappa^< = \int \frac{d\phi}{2\pi} \int_{E_-(k_R)}^0 dE \left(-\frac{\partial f^0}{\partial E}\right) \frac{(E-\mu)^2}{T} \times \sum_\nu N_{-\nu}(E)\, v_x^2(E,-\nu,\phi)\,\tau_{-\nu}(E). \tag{A8}$$

Therefore the Peltier coefficient can be expressed as

$$\alpha^> = \frac{1}{e}\int_0^\infty dE \left(-\frac{\partial f^0}{\partial E}\right) \frac{E-\mu}{T}\sigma^>(E) = \frac{1}{e}\int_0^\infty dE \left(-\frac{\partial f^0}{\partial E}\right) \frac{E-\mu}{T}\sigma(E) \tag{A9}$$

and

$$\alpha^< = \frac{1}{e}\int_{E_-(k_R)}^0 dE \left(-\frac{\partial f^0}{\partial E}\right) \frac{E-\mu}{T}\sigma^<(E) = \frac{1}{e}\int_{E_-(k_R)}^0 dE \left(-\frac{\partial f^0}{\partial E}\right) \frac{E-\mu}{T}\sigma(E), \tag{A10}$$

so that

$$\alpha = \frac{1}{e}\int_{E_-(k_R)}^\infty dE \left(-\frac{\partial f^0}{\partial E}\right) \frac{E-\mu}{T}\sigma(E). \tag{A11}$$

Similarly, the themal conductivity is connected with the zero-temperature electrical conductivity as

$$\kappa^> = \left(\frac{k_B}{e}\right)^2 T \int_0^\infty dE \left(-\frac{\partial f^0}{\partial E}\right) \left(\frac{E-\mu}{k_BT}\right)^2 \sigma(E) \tag{A12}$$

and

$$\kappa^{<}=\left(\frac{k_B}{e}\right)^2 T\int_{E_-(k_R)}^{0} dE\left(-\frac{\partial f^0}{\partial E}\right)\left(\frac{E-\mu}{k_B T}\right)^2\sigma\left(E\right), \tag{A13}$$

so we have

$$\kappa=\left(\frac{k_B}{e}\right)^2 T\int_{E_-(k_R)}^{\infty} dE\left(-\frac{\partial f^0}{\partial E}\right)\left(\frac{E-\mu}{k_B T}\right)^2\sigma\left(E\right). \tag{A14}$$

[1] E. Cappelluti, C. Grimaldi, and F. Marsiglio, Phys. Rev. Lett. **98**, 167002 (2007).

[2] K. Tsutsui and S. Murakami, Phys. Rev. B **86**, 115201 (2012).

[3] B. Lv and Z. S. Ma, Phys. Rev. B **87**, 045305 (2013).

[4] S. V. Eremeev, I. A. Nechaev, Yu. M. Koroteev, P. M. Echenique, and E. V. Chulkov, Phys. Rev. Lett. **108**, 246802 (2012); S. V. Eremeev, I. P. Rusinov, I. A. Nechaev, and E. V. Chulkov, New J. Phys. **15**, 075015 (2013).

[5] G. Landolt, S. V. Eremeev, Y. M. Koroteev, B. Slomski, S. Muff, T. Neupert, M. Kobayashi, V. N. Strocov, T. Schmitt, Z. S. Aliev, M. B. Babanly, I. R. Amiraslanov, E. V. Chulkov, J. Osterwalder, and J. H. Dil, Phys. Rev. Lett. **109**, 116403 (2012); G. Landolt, S. V. Eremeev, O. E. Tereshchenko, S. Muff, B. Slomski, K. A. Kokh, M. Kobayashi, T. Schmitt, V. N. Strocov, J. Osterwalder, E. V. Chulkov, and J. Hugo Dil, New. J. Phys. **15**, 085022 (2013).

[6] A. Crepaldi, L. Moreschini, G. Autes, C. Tournier-Colletta, S. Moser, N. Virk, H. Berger, P. Bugnon, Y. J. Chang, K. Kern, A. Bostwick, E. Rotenberg, O. V. Yazyev, and M. Grioni, Phys. Rev. Lett. **109**, 096803 (2012).

[7] M. Sakano, M. S. Bahramy, A. Katayama, T. Shimojima, H. Murakawa, Y. Kaneko, W. Malaeb, S. Shin, K. Ono, H. Kumigashira, R. Arita, N. Nagaosa, H. Y. Hwang, Y. Tokura, and K. Ishizaka, Phys. Rev. Lett. **110**, 107204 (2013).

[8] I. P. Rusinov, I. A. Nechaev, S. V. Eremeev, C. Friedrich, S. Blugel, and E. V. Chulkov, Phys. Rev. B **87**, 205103 (2013).

[9] J. Nitta, T. Akazaki, H. Takayanagi, and T. Enoki, Phys. Rev. Lett. **78**, 1335 (1997).

[10] L. Wu, J. Yang, S. Wang, P. Wei, J. Yang, W. Zhang, and L. Chen, Appl. Phys. Lett. **105**, 202115 (2014).

[11] W. Ming, Z. F. Wang, M. Zhou, and F. Liu, arXiv:1505.05073v1.

[12] C. Grimaldi, Phys. Rev. B **72,** 075307 (2005).

[13] A. Dyrdal, M. Inglot, V. K. Dugaev, and J. Barnas, Phys. Rev. B **87**, 245309 (2013).

[14] C. Xiao, D. P. Li, and Z. S. Ma, arXiv:1506.00203.

[15] B. Lv, C. Zhang, and Z. S. Ma, Phys. Rev. Lett. **108**, 077002 (2012).

[16] M. I. Alomar, L. Serra, and D. Sanchez, Phys. Rev. B **91**, 075418 (2015).

[17] G. E. W. Bauer, E. Saitoh, and B. J. van Wees, Nat. Mater. **11**, 391 (2012).

[18] SK. F. Islam and T. K. Ghosh, J. Phys.: Condens. Matter **24** 345301 (2012).

[19] J. M. Ziman, Principles of the Theory of Solids (Cambridge University Press, Cambridge, 1972).

[20] K. Vyborny, A. A. Kovalev, J. Sinova, and T. Jungwirth, Phys. Rev. B **79**, 045427 (2009).

[21] N. A. Sinitsyn, J. Phys.: Condens. Matter **20**, 023201 (2008).

[22] S. G. Novokshonov and A. G. Groshev, Phys. Rev. B, **74** 245333 (2006).

[23] M. Trushin and J. Schliemann, Phys. Rev. B **75**, 155323 (2007).

[24] L. Ye, J. G. Checkelsky, F. Kagawa, and Y. Tokura, Phys. Rev. B **91**, 201104(R) (2015).

[25] C.-R.Wang, J.-C. Tung, R. Sankar, C.-T. Hsieh, Y.-Y. Chien, G.-Y. Guo, F. C. Chou, and W.-L. Lee, Phys. Rev. B **88**, 081104(R) (2013).

[26] W. E. Chickering, J. P. Eisenstein, and J. L. Reno, Phys. Rev. Lett. **103**, 046807 (2009).